NOAA Technical Memorandum OAR GSL-67
https://doi.org/10.25923/f6a8-bc75

A Description of the MYNN Surface-Layer Scheme

Joseph B. Olson, Tanya Smirnova, Jaymes S. Kenyon, David D. Turner,
John M. Brown, Weizhong Zheng, and Benjamin W. Green

June 2021

National Oceanic and Atmospheric Administration
Oceanic and Atmospheric Research
Global Systems Laboratory
Boulder, CO

NOAA Technical Memorandum OAR GSL-XXX
https://doi.org/10.25923...

A Description of the MYNN Surface-Layer Scheme

[1]Joseph B. Olson, [1,2]Tanya Smirnova, [1,2]Jaymes S. Kenyon, [1]David D. Turner,
[1]John M. Brown, [3]Weizhong Zheng, and [1,2]Benjamin W. Green

[1]National Oceanic and Atmospheric Administration, Global Systems Laboratory (NOAA/GSL)
[2]Cooperative Institute for Research in Environmental Sciences (CIRES) and NOAA/GSL
[3]National Oceanic and Atmospheric Administration, National Center for Environmental Prediction, Environmental Modeling Center (NOAA/NCEP/EMC), and I.M. Systems Group, Inc.

Funding Sources
This work was provided by many sources, each helping to develop different components of the MYNN surface-layer scheme. These agencies/programs include NOAA's Atmospheric Science for Renewable Energy (ASRE) program, the Federal Aviation Administration (FAA), and NOAA's Next Generation Global Prediction System (NGGPS). The views expressed are those of the authors and do not necessarily represent the official policy or position of any funding agency.

National Oceanic and Atmospheric Administration/Oceanic and Atmospheric Research/
Global Systems Laboratory/Earth Prediction Advancement Division
Boulder, Colorado

U.S. Department of Commerce
Gina Raimondo, Secretary

National Oceanic and Atmospheric Administration
Neil Jacobs, Performing the duties of Under Secretary of Commerce for Oceans and Atmosphere

Office of Oceanic and Atmospheric Research
Craig McLean, Assistant Administrator

A Description of the MYNN Surface-Layer Scheme

June 2021

Contents

1. Introduction

The surface-layer scheme controls the degree of coupling between the model surface and the atmosphere. Traditionally, surface-layer schemes have been developed to be paired with certain planetary boundary layer (PBL) schemes, but this singular pairing is too narrow in scope for modern physics suites, since the surface-layer physics should also be well integrated with the land-surface model (LSM), gravity-wave drag scheme, and ocean wave model. The expansion of model complexity, such as the inclusion of subgrid-scale landuse variations, vertically distributed sources of drag [e.g., wind farm drag (Fitch *et al*. 2013), small-scale gravity wave drag (Steeneveld *et al*. 2008) and topographic form drag (Beljaars *et al*. 2004)], requires that the surface-layer scheme be developed within a broader context so assumptions made across all model components are physically consistent.

The surface-layer scheme described here was originally developed for the Mellor–Yamada–Nakanishi–Niino (MYNN)-Eddy Diffusivity-Mass Flux (EDMF) scheme (Nakanishi and Niino 2009, Olson *et al*. 2019) within the Advanced Research version of the Weather Research and Forecasting Model (WRF-ARW) (Skamarock *et al*. 2019). Earlier versions of this scheme have been used in NOAA's operational Rapid Refresh (RAP; Benjamin *et al*. 2016) and High-Resolution Rapid Refresh (HRRR) forecast systems since 2014. During this time, the scheme has undergone significant development in tandem with other components in the RAP/HRRR forecast systems. More recently, several new features have been added in order to accommodate different capabilities in the Common Community Physics Package (CCPP) (Firl *et al*. 2020), which is integrated with the FV3 model (Harris *et al*. 2020). This new version of the surface-layer scheme is a candidate to be used in the Rapid Refresh Forecast System (RRFS), which is a component of NOAA's emerging Unified Forecast System, and a successor to the RAP/HRRR forecast systems.

Traditional to WRF-ARW, the fluxes and diagnostics are calculated in the surface-layer scheme, although they are often overwritten later by the LSM or ocean model and dedicated diagnostic modules. Regardless, this document will describe how the fluxes and diagnostics are computed within this MYNN surface-layer scheme. Note that bypass switches have been added to the CCPP version of this surface-layer scheme to avoid these redundant calculations, but these switches have not yet been included in WRF-ARW versions.

In the real atmosphere, the surface layer is considered to be the lowest ~10% of the planetary boundary layer, where the turbulent fluxes are approximately constant with height (Stull 1988). In the model, the surface-layer scheme only regulates the heat, moisture, and momentum exchanges between the surface and the lowest model level—but not necessarily throughout the entire surface layer. This requires PBL schemes to properly parameterize surface layer turbulent fluxes that are consistent with the surface layer physics. This requirement is further complicated by the sensitivity of the surface heat and moisture fluxes and near-surface winds to the height of the lowest model level, which has recently been highlighted in several studies (e.g., Wei *et al*. 2001; Zängl *et al*. 2008; Shin *et al*. 2012; Lee *et al*. 2019). This sensitivity is not studied further here, but we note that this MYNN surface-layer scheme has been primarily developed within a model configuration that places its lowest mass level at 5-10 m above the surface, depending on

the height of the terrain. This configuration allows for a proper representation of surface-layer physics for most boundary layers deeper than ~50 m, but may be too coarse to properly represent very stable boundary layers, which likely have surface layer depths < 5 m. In contrast, with this shallow of a first model layer, some surface roughness elements (i.e., trees and buildings) may extend through the depth of the first model level (maybe even multiple levels). This has motivated the incorporation of elevated sources of drag (mentioned above) in order to resist the temptation to represent all forms of drag within this surface-layer scheme.

The surface layer physics represented by this scheme utilizes the traditional Monin-Obukhov stability theory (MOST) (Monin and Obukhov 1954), which is not novel but still represents a respectable performance benchmark. MOST has known deficiencies; e.g., it does not account for intermittent turbulence associated with large eddies, transient gravity waves, or meandering flows in very stable layers, nor does it account for the effects of sloped terrain and suffers from self-correlation of key non-dimensional variables (Andreas and Hicks 2002; Nieuwstadt 1984; Sorbjan 2006; Foken 2006; Mahrt 2007, 2008, 2010; Sun *et al*. 2020). Most of these shortcomings linger as unsolved problems for future surface layer physics development. Some of these problems will be discussed later.

2. General Design

The MYNN surface-layer scheme is built in a modular sense, which allows for flexible testing of a variety of different subcomponents. The specific subcomponents that exploit this modular design include the specification of the surface roughness lengths, the scalar roughness lengths, and the flux-profile relationships (a.k.a. stability functions). The configuration options for testing different forms of these subcomponents will be discussed below.

2.1 Bulk-Richardson number

The first step within the surface-layer scheme is to compute the bulk-Richardson number,

$$Ri_b = \frac{gz_1}{\theta_1}\frac{\theta_{v1}-\theta_{v0}}{U_1^2}, \quad (1)$$

where g is the acceleration due to gravity, z_1 is the height of the first mass-level, θ_1 and θ_{v1} are the potential temperature and the virtual potential temperature, respectively, of the air in the lowest model layer, θ_{v0} is the virtual potential temperature at the surface, and U_1 is the wind speed in the lowest model layer. To prevent singularities in Ri_b in the limit of vanishing wind speeds, three supplemental conditions to the background wind speeds are applied:

(1) in convective conditions, U_1 is not allowed to go below the convective velocity following Beljaars (1995) and Deardorff (1970), $w_* = \beta\left(\frac{g}{\theta_1} z_i \overline{w'\theta_v'}\right)^{1/3}$, where $\beta = 1.25$, z_i is the boundary layer height, and $\overline{w'\theta_v'}$ is the surface buoyancy flux;

(2) for mesoscale model applications with grid spacing (Δx) > 5000 m, there is assumed to be some background wind associated with subgrid-scale heterogeneities such as variations in cloud cover, terrain, landuse, etc. (Mahrt and Sun 1995), suggesting a lower limit of $U_{SG} = 0.32\left[MAX(\frac{\Delta x}{5000} - 1, 0)\right]^{1/3}$;

(3) in other conditions/configurations, U_1 is assumed to have a lower limit of 0.1 m s^{-1}.

2.2 Roughness lengths

The second step involves calculating the surface aerodynamic roughness lengths, z_0, and the scalar roughness lengths for heat and moisture (z_t and z_q respectively) over land, water, and snow/sea-ice. Over land, z_0 is typically a function of landuse type, which is specified by tables corresponding to various datasets and commonly vary for each land-surface model. There are some exceptions: (1) with *iz0tlnd* = 4 (GFS option), which will respecify z_0 for certain landuse types in the surface layer code, and (2) there is a z_0 dependence on both greenness fraction (for cropland) and snow depth in the RUC LSM (Smirnova *et al.* 2016). Once z_0 is known, the scalar roughness lengths can be determined (described below).

2.2.1 Land

For *iz0tlnd* = 0 (default), the form of Zilitinkevich (1995) is used:

$$z_t = z_0 exp\left[-kC_{Zil}\left(\frac{u_* z_0}{\nu}\right)^{1/2}\right], \quad (2)$$

where k is the von Karman constant (= 0.4), C_{Zil} is a free parameter set to 0.085, u_* is the friction velocity (defined below), and ν is the kinematic viscosity, which varies with temperature according to Andreas (1989). For this form, $z_q = z_t$.

For *iz0tlnd* = 1, the form of Zilitinkevich (1995) is also used, but C_{Zil} becomes dependent upon z_0 according to Chen and Zhang (2009):

$$C_{Zil} = 10^{(-kz_0/0.07)}. \quad (3)$$

This form also assumes $z_q = z_t$.

For *iz0tlnd* = 2, a modified form from Yang *et al*. (2002 and 2008) and Chen *et al*. (2010) is used. Although this form was originally designed for arid regions with bare soil, it is modified here to perform over a broader spectrum of landuse types. The original formulation relates z_t to u_* and the temperature scale, θ_* (a.k.a. friction temperature, defined in section 2.5):

$$z_t = h_t exp\left(-\beta_Y u_*^{1/2} {\theta_*}^{1/4}\right), \quad (4)$$

where $h_t = Re_c \nu / u_*$, the critical Reynolds number (Re_c) is taken as 70, and θ_* is bounded to be positive. The parameter β_Y was originally set at 10 (Yang *et al*. 2002), but was revised to 7.2 (Yang *et al*. 2008). Their form typically varies the ratio z_0/z_t by several orders of magnitude (10^{-4} to 10^0). The version implemented in the MYNN surface-layer scheme uses a further modified β_Y set to 1.5, a variable Re_c [= 691 + 170$ln(z_0)$], and the exponent on θ_* in Eq. (4) was changed to 1.0, since we found z_t was reduced too much for low-to-moderate positive heat fluxes. With these changes, z_t generally varies similarly to the Zilitinkevich (1995) form (refer to Eq. 2) with C_{Zil} = 0.1 for very small or negative surface heat fluxes, but can behave similarly to C_{Zil} = 0.2 for very large positive surface heat fluxes (common over bare soil/desert). For this form, $z_q = z_t$.

For *iz0tlnd* = 3, a constant thermal roughness length from Garratt (1992) is used:

$$z_t = \frac{z_0}{e^2} \approx \frac{z_0}{7.4}, \quad (5)$$

where *e* is Euler's number. This simple form was the default version when the MYNN surface-layer scheme was originally implemented into WRF-ARW (circa 2009), but is now maintained for comparisons to historical configurations or use in idealized model configurations. For this form, $z_q = z_t$.

For *iz0tlnd* = 4, a formulation from Zheng *et al*. (2012) is used, which utilizes green vegetation fraction (GVF) and a quadric method to represent z_t for all situations ranging from fully vegetated to bare soil. It implicitly includes the roughness Reynolds number (Re_*) and varies with seasons:#

$$z_t = z_{0eff} exp\left[-(1-GVF)^2 k C_{Zil}\left(\frac{u_* z_{0g}}{\nu}\right)^{1/2}\right], \quad (6)$$

where C_{Zil} is set to 0.8, z_{0g} is the roughness length over bare soil and is fixed at 0.01 m, and ν is the kinematic viscosity, which is set to 1.5×10^{-5} m^2 s^{-1}. This form also sets $z_q = z_t$.

An additional feature for *iz0tlnd* = 4 is the blended contribution of fully vegetated and bare soil on the effective roughness length, z_{0eff}, a weighted GVF-approach is used:

$$\ln(z_{0eff}) = (1-GVF)^2 \ln(z_{0g}) + [1-(1-GVF)^2]\ln(z_0). \quad (7)$$

As stated above, this form of thermal roughness length is used in tandem with the aerodynamic roughness lengths specified for this option. It is worth noting that this option has been tuned to improve both skin temperature and 2-m temperature in the operational GFS.

2.2.2 Water

Over water, z_0 is taken as a time-varying quantity, requiring it to be recalculated at each time step and the form of z_0 is controlled by the parameter *isftcflx*. For each option of *isftcflx*, there is an associated form of z_q and z_t.

For *isftcflx* = 0 (default), z_0, z_t, and z_q are specified by the COARE algorithm. However, there are two versions of the COARE bulk surface flux algorithm implemented in this surface-layer scheme, COARE 3.0 (Fairall *et al*. 2003) and COARE 3.5 (Edson *et al*. 2013). The hard-coded switch, *coare_opt*, should be set to 3.0 for COARE 3.0 (default) or set to 3.5 for COARE 3.5 (Edson *et al*. 2013). Note that the parameter *coare_opt* is declared as a REAL (not INTEGER) variable; if erroneously set, it will default to COARE 3.5.

The aerodynamic roughness lengths for COARE 3.0 are a function of u_* and the 10-m wind speed, U_{10}, with a variable Charnock parameter:

$$C_{cz} = C_{cz0} + 0.007\left(\frac{U_{10}-10}{8}\right), \quad (8)$$

where $C_{zc0} = 0.011$ and U_{10} is bounded between 10 and 18 m s^{-1}, so C_{cz} varies from 0.011 to 0.018. C_{cz} then appears in the commonly used equation for z_0:

$$z_0 = 0.11\frac{\nu}{u_*} + C_{cz}\frac{u_*^2}{g}, \quad (9)$$

where the first term on the right-hand side represents roughness lengths in the smooth sea surface limit, following Smith (1988), and the second term is the same form as in Charnock (1955). The thermal and moisture roughness lengths are a function of the Reynolds number ($Re = U_1 * z_0 / \nu$):

$$z_t = z_q = 5.5 \times 10^{-5} Re^{-0.6}. \quad (10)$$

The aerodynamic roughness lengths for COARE 3.5 are specified similarly to COARE 3.0, but the Charnock parameter varies more strongly with respect to wind speed:

$$C_{cz} = C_{cz0} + 0.017U_{10}, \quad (11)$$

where $C_{cz0} = -0.005$, U_{10} is bounded to be ≤ 19 m s^{-1}, and C_{cz} is bounded to be ≥ 0. C_{cz} is then used in Eq. (9) to compute z_0, just as in COARE 3.0. The thermal and moisture roughness lengths of COARE 3.5 are of similar form to COARE 3.0, but slightly changed to:

$$z_t = z_q = 5.8 \times 10^{-5} Re^{-0.72}. \quad (12)$$

For *isftcflx* = 1, z_0 is specified similar to Davis *et al*. (2008):

$$z_0 = \left(1 - \left(\frac{u_*}{1.06}\right)^{0.3}\right)\left(0.011\frac{u_*^2}{g} + 1.59 \times 10^{-5}\right) + \left(\frac{u_*}{1.06}\right)^{0.3}\left(10e^{-9.5u_*^{-\frac{1}{3}}} + 0.11\frac{\nu}{u_*}\right), \quad (13)$$

which is an updated form of Donelan *et al*. (2004) but has evolved even further over the years (Green and Zhang 2013). z_0 is bounded by 1.27×10^{-7} m and 2.85×10^{-3} m. The thermal and moisture roughness lengths are specified by the COARE algorithm as chosen by *coare_opt*.

For *isftcflx* = 2, z_0 is also specified according to Eq. (13), but the thermal and moisture roughness lengths are specified according to Garratt (1992), respectively as

$$z_t = z_0 e^{(2-2.48*Re^{1/4})} \quad (14a)$$

and

$$z_q = z_0 e^{(2-2.28*Re^{1/4})}. \quad (14b)$$

For this form, z_t and z_q are bounded between 2.0×10^{-9} and 5.5×10^{-5} m.

For *isftcflx* = 3, z_0 is specified according to Taylor and Yelland (2001), which attempts to link the roughness length to an estimate of the steepest waves:

$$z_0 = 1200 h_s \left(\frac{h_s}{L_p}\right)^{4.5}, \quad (15)$$

where $h_s = 0.0248(U_{10})^2$ is the significant wave height, $L_p = g(T_p)^2/(2\pi)$ is the wavelength associated with the peak of the wave frequency–size distribution, and $T_p = 0.279U_{10}$ is the associated dominant wave period. The thermal and moisture roughness lengths are specified by the COARE algorithm as chosen by *coare_opt*.

For *isftcflx* = 4, z_0 is calculated by a polynomial fit, blending the form of COARE 3.5 in low–moderate wind speeds with observational data in tropical-storm conditions to better match the observed drag coefficient (C_d)–U_{10} relationship across the wind-speed spectrum. The thermal and moisture roughness lengths are similarly calculated using a blended polynomial fit between the COARE algorithm and observational data. This work was done by Weiguo Wang and Bin Liu of NOAA-EMC and is a current option in the GFS surface-layer scheme.

2.2.3 Snow/Ice

There is currently only one bulk-flux algorithm for snow/ice. This form comes from Andreas (2002) and Andreas *et al*. (2005). The first step of this algorithm is to compute a z_0 for snow:

$$z_0 = 0.135\frac{\nu}{u_*} + 0.035\frac{u_*^2}{g}\left\{5exp\left[-\left(\frac{u_*-0.18}{0.10}\right)^2\right] + 1\right\}. \quad (16)$$

Note that this particular estimate of z_0 is only used internally within this snow/ice bulk algorithm for estimating the roughness Reynolds number, $Re = U_1 * z_0 / \nu$, and does not replace the z_0 provided by the LSM for any other calculation. Re and z_0 are then used as input into a set of best-fit polynomial equations to solve for z_t and z_q (Andreas 2002).

2.3 Solving for the surface stability parameter ζ (= z/L)

The necessary parameters (i.e., Ri_b, z_0, and z_t) have been computed in steps 1 and 2. The next step is to solve for the non-dimensional surface stability parameter ζ (= z/L), where z is the height above the surface and L is the Obukhov length. This requires iterating over the following equation:

$$\zeta = Ri_b \frac{\left[ln\left(\frac{z_1+z_0}{z_0}\right) - \psi_M\left(\frac{z_1+z_0}{L}\right) + \psi_M\left(\frac{z_0}{L}\right)\right]^2}{\left[ln\left(\frac{z_1+z_0}{z_t}\right) - \psi_H\left(\frac{z_1+z_0}{L}\right) + \psi_H\left(\frac{z_t}{L}\right)\right]}, \quad (17)$$

where z_1 is the height of the first model half-level and $\psi_{M,H}$ is a stability function, which has been derived empirically (discussed in the following section). The iteration is required because ζ is a function of $\psi_{M,H}$ and vice versa.

In the MYNN surface-layer scheme, there are two methods to iterate over (17). The first method is a two-point secant algorithm, taken from the revised surface-layer scheme in WRF-ARW (Jiménez *et al*. 2012) but adapted for use when $z_t \neq z_0$. The second method is a "brute-force" approach, which requires a first-guess ζ from Li *et al*. (2010), which is an approximate analytical estimate of ζ, and then iterates back and forth between solving for ψ and ζ until convergence is achieved. In our experience, convergence is always achieved (for both options) within 20 iterations but can take more iterations in very stable conditions over land (Fig. 1). As a safeguard, in the event convergence is not achieved after 20 iterations, an estimate of z/L from Li *et al*. (2010) is used and the iteration is terminated. Both options produce an estimate of z/L with the same sign as Ri_b with a well-behaved monotonic increase of z/L with increasing Ri_b, so the flux-profile relationships (discussed in the following section) are never applied in stability regimes for which they are not intended [as discussed in Kumar and Sharan (2012)]. Note that there is no switch to choose between these two options; instead, the calls to each function are hard-coded, so a manual edit is necessary to change the default (brute-force method).

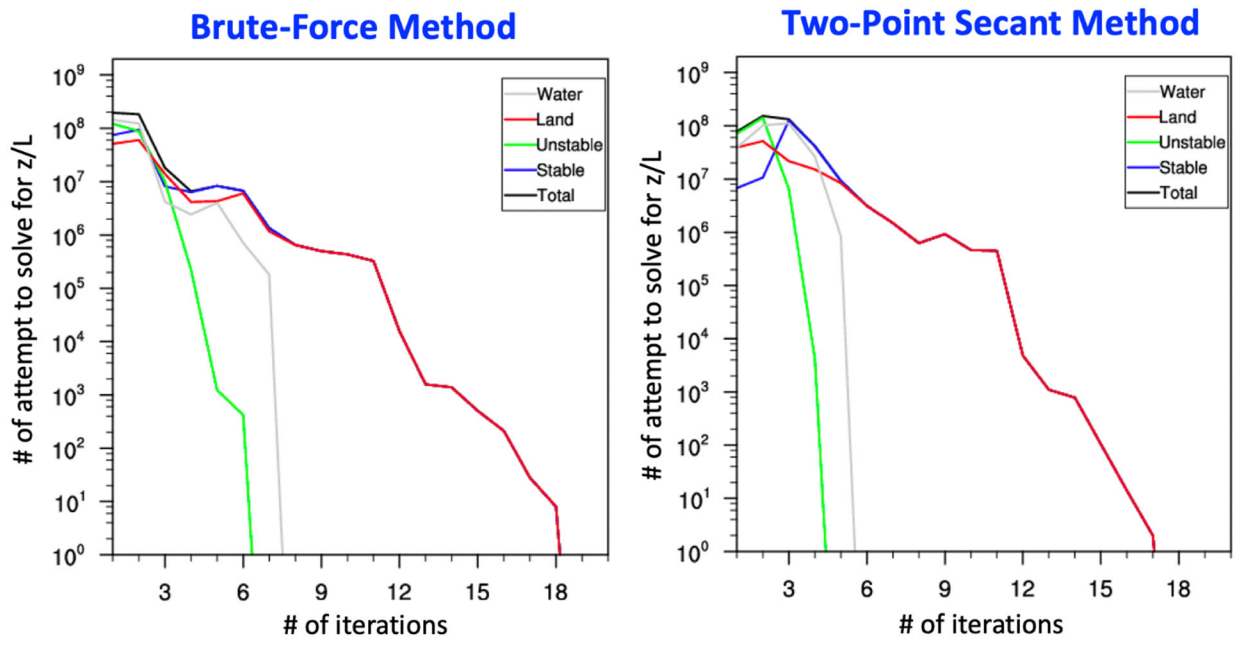

Figure 1. The total number of attempts to solve for z/L as a function of the number of iterations required to reach a converged solution for the "brute-force" (left) and two-point secant (right) methods. The number of attempts is also broken down into land vs water and unstable vs stable. These results are from a single HRRR forecast.

2.4 Stability Functions

The fourth step is to calculate values for the empirically-formulated stability functions for heat (ψ_H) and momentum (ψ_M), which are used in step 3 (above), but final values are not determined until after convergence is achieved in the iterative procedure described above. The forms of the stability functions are chosen by setting the hard-coded parameter *psi_opt*.

For *psi_opt* = 0 (default), the forms in unstable conditions ($\zeta = z/L < 0$) use Grachev *et al.* (2000). These are a blend of the classical "Kansas" forms (i.e., Paulson 1970, Dyer and Hicks 1970), valid for weakly unstable conditions ($-1 < \zeta < 0$):

$$\psi_{M-Kansas} = 2\,ln\left(\frac{1+x}{2}\right) + ln\left(\frac{1+x^2}{2}\right) - 2\,arctan(x) + \frac{\pi}{2}, \quad (18)$$

$$\psi_{H-Kansas} = 2\,ln\left[\frac{1}{2}\left(1+\sqrt{1-16\,\zeta}\right)\right], \quad (19)$$

where $x = (1-16\zeta)^{1/4}$, and a form that scales as $\zeta^{-1/3}$ in extreme unstable conditions ($\zeta \ll -1$) following Grachev and Fairall (1997):

$$\psi_{M,H-Grachev} = \frac{3}{2}ln\left(y^2+y+\frac{1}{3}\right) - \sqrt{3}\,arctan\left(2y+3^{-1/2}\right) + \frac{\pi}{\sqrt{3}}, \quad (20)$$

where $y = (1-34\zeta)^{1/3}$. Equations (18), (19), and (20) are then blended as a function of ζ by the following weighting function:

$$\psi_{M,H} = \frac{\psi_{M,H-Kansas} + \zeta^2\psi_{M,H-Grachev}}{1+\zeta^2}, \quad (21)$$

which gives good agreement with the standard Kansas-type expressions for near-neutral stratification and obeys the asymptotic convective limit (Grachev *et al.* 2000).

The stability functions for stable conditions use an updated form taken from Cheng and Brutsaert (2005), which extends the validity into very stable conditions [$z/L \sim O(10)$]:

$$\psi_M = -6.1\, ln\left\{\frac{z}{L} + \left[1 + \left(\frac{z}{L}\right)^{2.5}\right]^{1/2.5}\right\}, \tag{22}$$

$$\psi_H = -5.3\, ln\left\{\frac{z}{L} + \left[1 + \left(\frac{z}{L}\right)^{1.1}\right]^{1/1.1}\right\}. \tag{23}$$

Currently, the range of z/L is bounded between −20 and 20.

For *psi_opt* = 1, stability functions from the GFS surface-layer scheme are adopted. In unstable conditions ($\zeta = z/L < 0$), different forms of the similarity functions are used for weakly unstable/near-neutral and strongly unstable regimes:

$$\psi_M = \begin{cases} ln\left(\frac{z}{L}\right) + 2\sqrt{\frac{1}{\sqrt{-\frac{z}{L}}}} - 0.8776, & \frac{z}{L} < -0.5 \\ \frac{a_0\left(\frac{z}{L}\right) + a_1\left(\frac{z}{L}\right)^2}{\frac{z}{L} + b_1\left(\frac{z}{L}\right) + b_2\left(\frac{z}{L}\right)^2}, & \frac{z}{L} \geq -0.5 \end{cases} \tag{24}$$

$$\psi_H = \begin{cases} ln\left(\frac{z}{L}\right) - \frac{1}{2}\left(\frac{z}{L}\right) + 1.386, & \frac{z}{L} < -0.5 \\ \frac{a_{0h}\left(\frac{z}{L}\right) + a_{1h}\left(\frac{z}{L}\right)^2}{\frac{z}{L} + b_{1h}\left(\frac{z}{L}\right) + b_{2h}\left(\frac{z}{L}\right)^2}, & \frac{z}{L} \geq -0.5 \end{cases} \tag{25}$$

where $a_0 = -3.975$, $a_1 = 12.32$, $b_1 = -7.755$, $b_2 = 6.041$, $a_{0h} = -7.941$, $a_{1h} = 24.75$, $b_{1h} = -8.705$, $b_{2h} = 7.899$. The form for stable conditions is:

$$\psi_M = \psi_H = -a_s + ln(a_s + 1), \tag{26}$$

where $a_s = (1 + 20z/L)^{1/2}$.

When the scheme is configured to use the aerodynamic and scalar roughness lengths from the GFS (*iz0tlnd* = 4), under stable conditions, a stability parameter constraint $(z/L)_{lim}$ is introduced to prevent the land-atmosphere system from fully decoupling (Zheng *et al*. 2017):

$$\left(z/L\right)_{lim} = ln\left(z_1/z_0\right)/\left[2\alpha\left(1 - z_0/z_1\right)\right]. \tag{27}$$

Here z_1 is the height of the first model half-level, L is the Obukhov length, z_0 is the momentum roughness length, and $\alpha = 5$. Currently, the same bounds for z/L as used in *psi_opt* = 0 are applied here, but the upper-limit of z/L in Eq. (27) imposes a further constraint. Note that the impact of this limit is analogous to the limits imposed on the background wind speed (section 2.1) and the lower limit to u_* over land (see next section). That is, these limits are at least partially meant to mitigate the numerical problem of runaway cooling in the very stable surface layer (Mahrt 1998; Steeneveld *et al*. 2010).

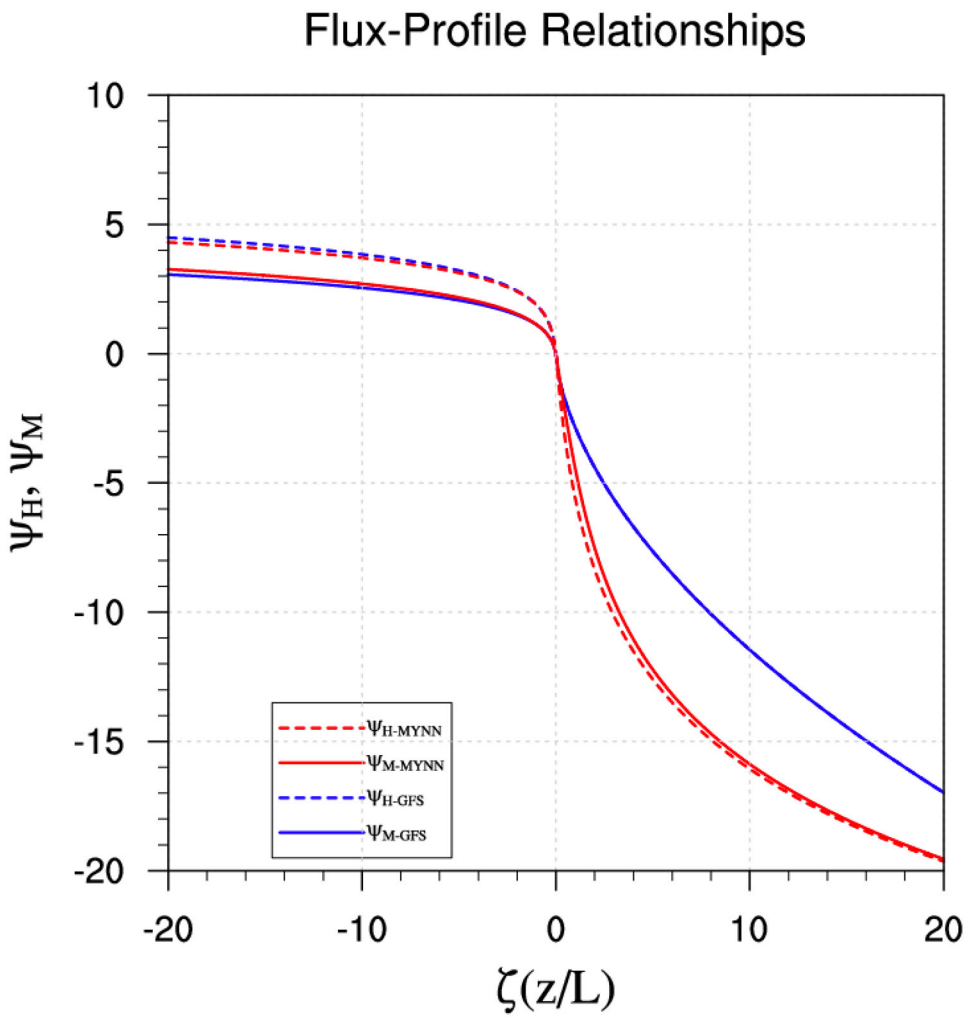

Figure 2. Flux-profile relationships as a function of surface stability parameter z/L. The form denoted as "MYNN" (red) are used for psi_opt = 0 (default) and the form denoted as "GFS" (blue) are used for psi_opt = 1.

The two forms of ψ_H and ψ_M are shown for comparison (Fig. 2). The two forms are very similar in the unstable regime, but the larger negative values of Cheng and Brutsaert (2005) (used when *psi_opt* = 0, default) will produce larger resistance (weaker coupling) between the surface and atmosphere in stable conditions.

2.5 Calculation of Surface Exchange Coefficients and Fluxes

The fifth step is the calculation of the surface momentum flux (τ, a stress, in kg m^{-1} s^{-2}), sensible heat flux (*HFX*, in W m^{-2}), and moisture flux (*QFX*, kg m^{-2} s^{-1}), which are expressed in terms of differences between variables at level model mass-level, z_1, (identified by the subscript '1') and the same variables at the surface (identified by the subscript '0', except for z_0, which is the aerodynamic roughness length):

$$\tau = \rho_1 C_M U_1^2 = \rho_1 u_*^2$$
$$HFX = \rho_1 c_p C_H U_1 (\theta_1 - \theta_0) \quad (28)$$

$$QFX = \rho_1 C_Q U_1 (qv_1 - qv_0),$$

where U_1 is the same wind speed used in the Ri_b calculation (Eq. 1), θ_0 and θ_1 are potential temperatures at the surface and first mass level respectively, and qv_0 and qv_1 are the mixing ratios at the surface and first mass level respectively. Note that these fluxes, if configured to be calculated in the surface layer (when *compute_flux* = True), will be overwritten by subsequent flux calculations made in the LSM or ocean models, but can still be calculated in the surface-layer scheme for idealized modeling configurations. The surface exchange coefficients, C_M, C_H, and C_Q are respectively expressed as:

$$C_M = \frac{k^2}{\left[ln\left(\frac{z_1+z_0}{z_0}\right) - \psi_M\left(\frac{z_1+z_0}{L}\right) + \psi_M\left(\frac{z_0}{L}\right)\right]^2}, \tag{29a}$$

$$C_H = \frac{k^2}{\left[ln\left(\frac{z_1+z_0}{z_0}\right) - \psi_M\left(\frac{z_1+z_0}{L}\right) + \psi_M\left(\frac{z_0}{L}\right)\right]\left[ln\left(\frac{z_1+z_0}{z_t}\right) - \psi_H\left(\frac{z_1+z_0}{L}\right) + \psi_H\left(\frac{z_t}{L}\right)\right]}, \tag{29b}$$

$$C_Q = \frac{k^2}{\left[ln\left(\frac{z_1+z_0}{z_0}\right) - \psi_M\left(\frac{z_1+z_0}{L}\right) + \psi_M\left(\frac{z_0}{L}\right)\right]\left[ln\left(\frac{z_1+z_0}{z_q}\right) - \psi_H\left(\frac{z_1+z_0}{L}\right) + \psi_H\left(\frac{z_q}{L}\right)\right]}. \tag{29c}$$

Note that the denominators in Eqs. (29) are sometimes referred to as "resistance" [see chapter 2 of Stensrud (2007) for an excellent discussion on this electrostatic analogy], where larger z_1, smaller roughness lengths (z_0, z_t and z_q), and/or positive net contribution of the ψ terms act to increase the resistance, thus reducing the exchanges between the surface and the atmosphere. Note that when $z_t = z_q$ (which is the case for most configurations), $C_H = C_Q$.

The friction velocity, friction temperature, and friction moisture, which have been used in section 2.2, are respectively calculated as follows:

$$u_* = \frac{kU_1}{\left[ln\left(\frac{z_1+z_0}{z_0}\right) - \psi_M\left(\frac{z_1+z_0}{L}\right) + \psi_M\left(\frac{z_0}{L}\right)\right]} = U_1 C_M^{1/2}, \tag{30}$$

$$\theta_* = \frac{k(\theta_1-\theta_0)}{\left[ln\left(\frac{z_1+z_0}{z_t}\right) - \psi_H\left(\frac{z_1+z_0}{L}\right) + \psi_H\left(\frac{z_t}{L}\right)\right]} = \frac{-HFX}{\rho\, c_p\, u_*}, \tag{31}$$

$$q_* = \frac{k(qv_1-qv_0)}{\left[ln\left(\frac{z_1+z_0}{z_q}\right) - \psi_H\left(\frac{z_1+z_0}{L}\right) + \psi_H\left(\frac{z_q}{L}\right)\right]} = \frac{-QFX}{\rho\, c_p\, u_*}. \tag{32}$$

Note that, in the MYNN surface-layer scheme, u_* is an average of values obtained at the present and previous timesteps. This averaging—a feature inherited by the MYNN from an earlier version of the Yonsei University (YSU) surface-layer scheme—is thought to improve computational stability, but this has not been proven as essential. Also, u_* is constrained to never become less than 0.005 m s^{-1} over land. However, due to the lower limit imposed on U_1 (in section 2.2), this limit on u_* is seldom required.

Lastly, there are alternative forms of the "exchange coefficients" for scalars in the surface layer code, which are also inherited from the YSU surface-layer scheme, but they have been retained because they may be used by other model components. These forms are essentially combinations of the exchange coefficients expressed in Eq. (29) and other parameters or variables. For completeness, these alternative forms and their relationships to the exchange coefficients expressed in Eq. (29) are:

$$FLHC = \frac{\rho c_p u_* k}{\left[ln\left(\frac{z_1+z_0}{z_t}\right) - \psi_H\left(\frac{z_1+z_0}{L}\right) + \psi_H\left(\frac{z_t}{L}\right)\right]} = \rho c_p C_H U_1, \tag{33}$$

$$FLQC = \frac{\rho u_* k}{\left[ln\left(\frac{z_1+z_0}{z_q}\right)-\psi_H\left(\frac{z_1+z_0}{L}\right)+\psi_H\left(\frac{z_q}{L}\right)\right]} = \rho C_Q U_1, \quad (34)$$

$$CHS = \frac{u_* k}{\left[ln\left(\frac{z_1+z_0}{z_t}\right)-\psi_H\left(\frac{z_1+z_0}{L}\right)+\psi_H\left(\frac{z_t}{L}\right)\right]} = C_H U_1. \quad (35)$$

These alternative forms are output by the MYNN surface-layer scheme in both WRF-ARW and CCPP/FV3.

2.6 Calculation of Diagnostics

The sixth step is to calculate the near-surface diagnostics. All of the diagnostic calculations are bypassed in the version of the MYNN surface-layer scheme in CCPP/FV3 by default (when *compute_diag* = False), since these diagnostics are computed in subsequent calls to other model components. Nonetheless, they are described below, since they may still be of use if the model (e.g., WRF) is run in an idealized mode, which may not utilize the other model components that compute the diagnostics.

2.6.1 10-m Wind Speed

The 10-m zonal and meridional wind components, *U10* and *V10*, respectively, are two-dimensional fields computed by using a neutral-log interpolation:

$$U10 = U_1 \ln(10/z_0)/\ln(z_1/z_0) \quad (36)$$

$$V10 = V_1 \ln(10/z_0)/\ln(z_1/z_0), \quad (37)$$

where U_1 and V_1 are the wind components valid at the middle of the lowest atmospheric model layer, z_1 is equal to half the depth of the first model layer, and z_0 is the aerodynamic roughness length. Note that prior to WRF–ARWv4.0, *U10* and *V10* were set equal to the wind components at the lowest model level if the height of the first model level (z_1) was $7 < z_1 < 13$ m.

2.6.2 2-m Temperature

The 2-m potential temperature calculation uses an interpolation between the surface potential temperature (θ_0) and the potential temperature at the first mass-level (θ_1), weighted by the ratio of the thermal resistances in the lowest 2 m and in the first model layer:

$$\theta_{2m} = \theta_0 + (\theta_1 - \theta_0)\frac{\left[ln\left(\frac{2+z_0}{z_t}\right)-\psi_H\left(\frac{2+z_0}{L}\right)+\psi_H\left(\frac{z_t}{L}\right)\right]}{\left[ln\left(\frac{z_1+z_0}{z_t}\right)-\psi_H\left(\frac{z_1+z_0}{L}\right)+\psi_H\left(\frac{z_t}{L}\right)\right]}. \quad (38)$$

Then, the 2-m absolute temperature is obtained via:

$$T_{2m} = \theta_{2m}\left(\frac{p_{sfc}}{100000}\right)^{R/c_p}, \quad (39)$$

where p_{sfc} is the pressure at the surface (in Pa), R is the dry gas constant, and c_p is the specific heat at constant pressure of dry air.

2.6.3 2-m Water Vapor Mixing Ratio

The 2-m water vapor mixing ratio, qv_{2m}, calculation uses an interpolation between the surface mixing ratio, qv_0, and the mixing ratio at the first mass-level, qv_1, weighted by the ratio of the moisture resistances in the lowest 2 m and in the first model layer:

$$qv_{2m} = qv_0 + (qv_1 - qv_0)\frac{\left[ln\left(\frac{2+z_0}{z_q}\right)-\psi_H\left(\frac{2+z_0}{L}\right)+\psi_H\left(\frac{z_q}{L}\right)\right]}{\left[ln\left(\frac{z_1+z_0}{z_q}\right)-\psi_H\left(\frac{z_1+z_0}{L}\right)+\psi_H\left(\frac{z_q}{L}\right)\right]}. \quad (40)$$

Over water, qv_0 is taken as the saturated water vapor mixing ratio. Over land, qv_0 comes out of land-surface model by solving the energy budget equation at the surface. The energy budget gives the relationship between two unknown variables: surface skin temperature and qv_0. If it is snow or ice then qv_0 is taken as the saturated water vapor mixing ratio, otherwise qv_0 is computed from the saturated mixing ratio and the soil moisture availability.

3. Communication with Other Model Components

3.1 Boundary Layer Scheme

Most boundary layer schemes require u_*, *HFX* [or $HFX/(\rho c_p)$], and *QFX* (or QFX/ρ) as input for lower boundary conditions. Some other schemes, such as the MYNN-EDMF (Olson *et al*. 2019) also require the Obukhov length, L (or z/L), to regulate the surface layer mixing length scales as well as the lower boundary condition for shear and buoyancy production of turbulent kinetic energy. The only variable computed by the boundary layer schemes that is needed as input to the MYNN surface-layer scheme at the following timestep is the planetary boundary layer height (z_i).

3.2 Land-Surface Model

Different LSMs require different input; for example, both Noah and RUC LSMs (Smirnova *et al*. 2016) will use the surface exchange coefficients calculated by the surface-layer scheme when solving the surface energy and moisture balances. However, Noah-MP (Niu *et al*. 2011, Yang *et al*. 2011) will discard these exchange coefficients and recalculate its own exchange coefficients within its iterative surface energy balance solver. This is an important distinction that must be considered when trying to diagnose the origin of biases in near-surface variables.

The LSMs will compute the surface moisture and skin temperature for input into the surface-layer scheme (on the following timestep). Although the MYNN surface-layer scheme has the capability to compute the surface stability parameter z/L, transfer coefficients, and the momentum and scalar fluxes (u_*, *HFX*, and *QFX*) over all grid points, the LSMs will recalculate the scalar fluxes over land grid points; the sea-ice models (uncoupled or coupled) will reevaluate the scalar fluxes over sea ice; and the ocean models (uncoupled or coupled) will overwrite *HFX* and *QFX* over water.

The LSMs, for example, the RUC LSM in CCPP, might request separate transfer coefficients for snow-free and snow-covered portions of the grid cells. This option will be provided by MYNN surface-layer scheme in its future revision.

3.3 Gravity Wave Drag Scheme

The MYNN surface-layer scheme is not dependent upon any fields from the gravity wave drag scheme in WRF–ARW or CCPP/FV3; however, both schemes can impact the momentum flux (drag) at the surface. Specifically, the blocking drag, the small-scale gravity wave drag (Steeneveld *et al*. 2008), and the topographic form drag (Beljaars *et al*. 2004) all impact the low-level winds, so this must be taken into context when making any adjustments in the model to improve low-level winds. The MYNN surface-layer scheme has been tuned to work with these drag components, so the characteristic biases of the low-level winds may be suboptimal if the scheme is used without the proper representation of these sources of drag.

3.4 Wave Model

The MYNN surface-layer scheme in CCPP/FV3 is capable of running with the WAVEWATCH III® wave model (Tolman 2008). In this configuration, z_0 is computed within the wave model and the calculation of z_0 is then bypassed in the surface-layer scheme. This ensures that only one of the two schemes will impact the momentum flux (drag) at the surface over the ocean.

4. Code Description

For context, the surface-layer scheme is called directly after the radiation and prior to the surface modules (land-surface, sea-ice, and sea-surface models). The surface-layer scheme and the surface modules collectively calculate the necessary input for the boundary-layer schemes (beyond the basic state variables); i.e., u_*, z/L, surface heat and moisture fluxes.

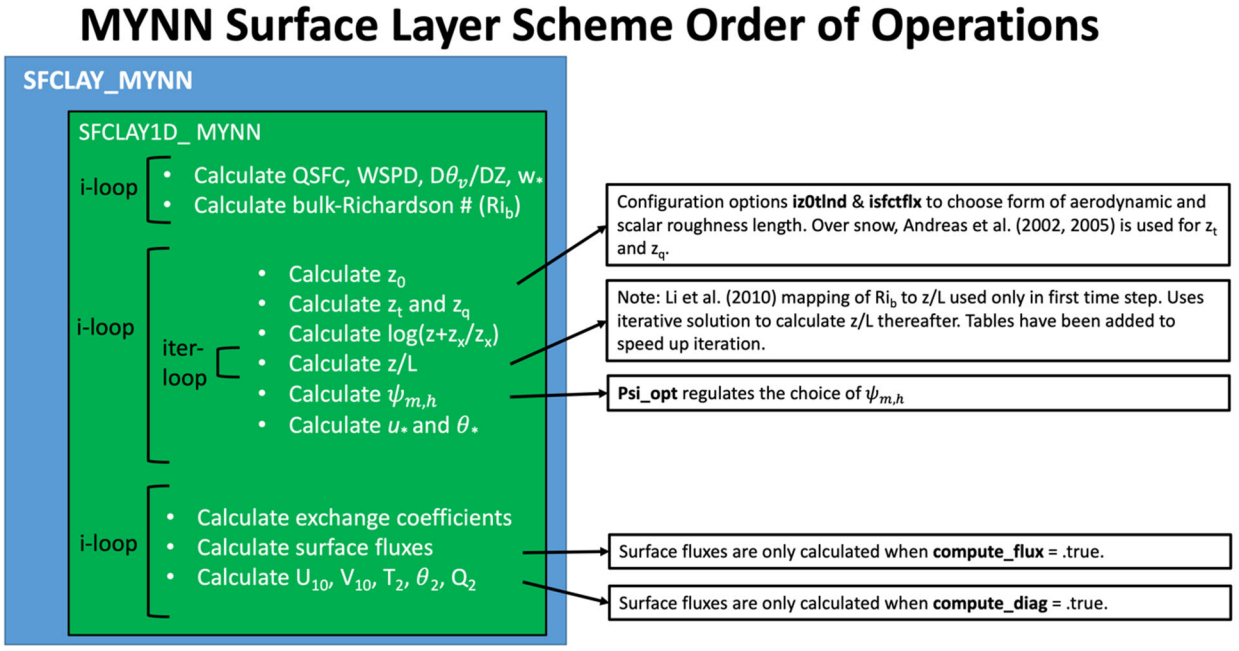

Figure 3. The order of operations within the MYNN surface layer scheme.

Within the MYNN surface-layer scheme, there is a dependency check for the first timestep. If true, several arrays are initialized at every surface grid point, represented by *i*. This is done because (1) some variables are calculated in schemes called after the surface layer call, and (2) some variables are used within iterative processes and may not be specified until later in the surface-layer scheme. We describe the main order of operations (Fig. 3) and highlight relevant subroutines below:

- Calculate the surface bulk-Richardson number.
- Either use the input aerodynamic roughness lengths **over land** (default) or re-specify the aerodynamic roughness length for *iz0tlnd* = 4:
    - Subroutine **GFS_Z0_LND** is used to re-specify z_0 for some landuse types.
- Calculate the aerodynamic roughness lengths **over water** according to specified value for *isftcflx*:
    - If *coare_opt* = 3.0, then subroutine **CHARNOCK_1955** is used for *isftcflx* = 0. The name of this subroutine is misleading in that it actually uses a variable Charnock parameter according to COARE 3.0 (Fairall *et al*. 2003). If *coare_opt* = 3.5, then subroutine **EDSON_ETAL_2013** is used for *isftcflx* = 0.
    - Subroutine **DAVIS_ETAL_2008** is used for *isftcflx* = 1
    - Subroutine **DAVIS_ETAL_2008** is again used for *isftcflx* = 2
    - Subroutine **TAYLOR_YELLAND_2001** is used for *isftcflx* = 3
    - Subroutine **GFS_Z0_OCN** is used for *isftcflx* = 4
- Calculate the thermal and moisture roughness lengths **over land** according to specified value for *iz0tlnd*:
    - Subroutine **ZILITINKEVICH_1995** is used for *iz0tlnd* = 0.
    - Subroutine **ZILITINKEVICH_1995** is used for *iz0tlnd* = 1, but an alternative form of C_{zil} is used from Chen and Zhang (2009).
    - Subroutine **YANG_2008** is used for *iz0tlnd* = 2
    - Subroutine **GARRATT_1992** is used for *iz0tlnd* = 3
    - Subroutine **GFS_ZT_LND** is used for *iz0tlnd* = 4
- Calculate the thermal and moisture roughness lengths **over water** according to specified value for *isftcflx*:
    - Subroutine **FAIRALL_ETAL_2003** or **FAIRALL_ETAL_2014** (depending on choice of COARE_OPT) is used for *isftcflx* = 0. Note that there was an expected update to COARE 3.5 scalar fluxes in 2014, but no publication detailing this update has been found, so the name of the subroutine "FAIRALL_ETAL_2014" is misleading.
    - Subroutine **FAIRALL_ETAL_2003** or **FAIRALL_ETAL_2014** (depending on choice of COARE_OPT) is used for *isftcflx* = 1.
    - Subroutine **GARRATT_1992** is used for *isftcflx* = 2
    - Subroutine **FAIRALL_ETAL_2003** or **FAIRALL_ETAL_2014** (depending on choice of COARE_OPT) is used for *isftcflx* = 3
    - Subroutine **GFS_ZT_OCN** is used for *isftcflx* = 4
- If there is a non-zero snow fraction or sea-ice fraction in the grid cell, calculate the thermal and moisture roughness lengths for snow/ice:

    - Subroutine **ANDREAS_2002** uses the form from Andreas (2002) and Andreas *et al*. (2005).
- Calculate all logarithmic terms [i.e., $ln((z_{x1} + z_0)/z_{x2})$], where z_{x1} can be the height of the first mass-level, 2 m or 10 m and z_{x2} can be either z_0, z_t or z_q) in preparation for the iterative solver.
- Solve for z/L using one of the two different iterative methods that exist in the code. Note that these options are hard-coded, so altering them will require commenting out one and uncommenting out the other.
    - Function **ZOLRI**: solves for z/L using the "two-point secant" method.
    - Function **ZOLRIB**: solves for z/L using the "brute-force" method (default).
- Calculate the stability functions ψ_H and ψ_M for the exchange coefficients as well as those used for the diagnostics ($\psi_{M\text{-}10m}$ and $\psi_{H\text{-}2m}$). Note that different form can be chosen by the internal (hard-coded) parameter *psi_opt*.
- Calculate u_*, θ_*, and q_*.
- Compute the transfer coefficients.
- If *compute_flux* = true (set to false by default), compute the surface heat and moisture fluxes.
- If *compute_diag* = true (set to false by default), compute the 2-m temperature, 2-m mixing ratio, and 10-m u- and v-wind components.

5. Summary and Future Work

The original MYNN surface-layer scheme was derived from the YSU surface-layer scheme at about the time when the MYNN PBL scheme was implemented into WRF–ARWv3.1 (in 2009). This original version had very little customization for compatibility with the MYNN PBL scheme and contained many bugs (some were discussed in Jiménez *et al*. 2012). Over the following decade, the MYNN surface-layer scheme was developed within a broader context to become better interfaced with the MYNN PBL scheme and other model components, such as the land-surface models, gravity wave drag scheme, and a wave model. It has also been expanded to include many options for a variety of operational and research applications. In 2014, the MYNN surface-layer scheme (along with the MYNN PBL) was incorporated into NOAA's operational RAP/HRRR forecast system and has undergone further development as forecast biases have been better quantified over time. These innovations notwithstanding, there are still several opportunities for improvement:

5.1 Embedding the surface layer physics inside the LSM's iterative surface energy balance solver

The surface exchange coefficients calculated in the surface-layer scheme are consistent with the mean state variables within the surface-atmospheric interface at the beginning of a timestep, but as they are used in the LSM's iterative solver to obtain a new surface energy balance, it is likely that they may no longer be consistent with the final (or intermediate) state. To obtain a more accurate solution, it may be necessary to embed the surface layer physics within the LSM, such that the surface exchange coefficients are updated within the iteration to obtain the new surface

energy balance (as implemented in the Noah-MP LSM). This semi-implicit approach has the potential to improve the likelihood of convergence towards a physically realistic solution, which can be especially problematic in transition periods when the equilibrium state changes significantly between timesteps. This approach may require a more efficient bulk-flux algorithm than the traditionally used Monin-Obukhov methods (see topic ii. below).

5.2 Richardson number-dependent functions to replace Monin-Obukhov bulk-flux algorithm

Integrating the surface layer physics into the LSM to improve the solution of the surface energy balance may require more efficient bulk-flux algorithm for obtaining updated surface exchange coefficients. Integrating traditional Monin-Obukhov methods into the surface energy balance solver will effectively add an iterative method inside another iterative solver, which may be computationally expensive, especially for future scheme designs that may require multiple solutions for each subgrid-scale landuse or soil-type within a grid cell. A non-iterative technique, such as a Richardson number-based bulk flux algorithm (e.g., Lee and Buban 2020, Deardorff 1972) has the potential to be both computationally efficient and avoid some of the caveats associated with Monin-Obukhov stability theory, such as self-correlation (e.g., Andreas and Hicks 2002, Foken 2006). However, work is continuing to develop a bulk Richardson number approach that seamlessly spans from very unstable to very stable conditions and is applicable to all landuse types.

5.3 Integrate the capability to account for subgrid-scale variability

There is an ongoing effort to improve the handling of subgrid-scale variability in surface properties into LSMs (e.g. He and Ohara 2019), so it is vital that companion development must occur in the surface-layer schemes. The types of heterogeneity may include landuse, soiltype, shading, topographic slopes, etc. These heterogeneities can result in significant variations in surface fluxes within the area covered by a single grid cell, which may drive a highly variable atmospheric turbulent response. The fractional land grid option (*frac_grid*), already implemented in CCPP, requires up to three sets of transfer coefficients for the single grid cell that contains fractions of three surface categories: land, sea-ice, or water (ocean or lakes) or a combination of any two of them. Future developments within the LSMs might require the MYNN surface-layer scheme to provide, for example, separate sets of transfer coefficients for snow-free and snow-covered portions of land or ice fractions of a grid cell. Additionally, the MYNN surface-layer scheme may provide transfer coefficients for several dominant landuse categories within the land portion of a grid cell. This detailed representation of the distribution of surface fluxes within a grid cell is a necessary prerequisite before these variations can be better represented within the boundary layer schemes.

Acknowledgments. We are grateful to the National Center for Atmospheric Research (NCAR) Mesoscale and Microscale Meteorology (MMM) Laboratory (http://www.mmm.ucar.edu/wrf/users), which is responsible for the WRF-ARW and MPAS models. We are specifically grateful for help from Jimy Dudhia, Wei Wang, Dave Gill. We are also grateful to the CCPP developers, especially Dominikus Heinzeller (NOAA-GSL) and Grant Firl (NCAR-DTC) for their help integrating, testing, and maintaining this code in their respective repositories.

Appendix: Summary of MYNN Surface-Layer Scheme Configuration Options

Switch/Option	Value	Description
iz0tlnd	0	Zilitinkevich (1995) with C_{Zil} set to 0.085 (default)
	1	Zilitinkevich (1995), but with C_{Zil} modified according to Chen and Zhang (2009)
	2	Modified Yang *et al*. (2002, 2008) - generalized for all landuse
	3	Constant $z_t = z_0/7.4$ (original form; Garratt 1992)
	4	(GFS) - Zheng *et al*. (2012) green vegetation fraction dependent
isftcflx	0	z_0, z_t and z_q from the COARE algorithm. Set *COARE_OPT* (below) to 3.0: Fairall *et al*. (2003), default 3.5: Edson *et al*. (2013)
	1	z_0 based off Davis *et al*. (2008), z_t and z_q from COARE 3.0/3.5
	2	z_0 based off Davis *et al*. (2008), z_t and z_q from Garratt (1992)
	3	z_0 from Taylor and Yelland (2004), z_t and z_q from COARE 3.0/3.5
	4	(GFS) - z_0, z_t and z_q from blended COARE3.5/HWRF (chosen by setting *sfc_z0_type*)
coare_opt	3.0	COARE v3.0 - Fairall *et al*. (2003), default
	3.5	COARE v3.5 - Edson *et al*. (2013)
psi_opt	0	Stability functions from Cheng and Brutsaert (2005) in stable conditions and the blended form of Grachev *et al*. (2000) for unstable conditions (default)
	1	(GFS).
isfflx	0	Set surface fluxes to zero. For idealized use only.
	1	Compute (non-zero) transfer coefficients and fluxes.

Table 1. Description of the configuration options pertaining to the MYNN Surface-layer scheme.

References

Andreas, E. L., 1989: Thermal and size evolution of sea spray droplets. *CRREL Report 89-11, U.S. Army Corps of Engineers*. Pp. 48.

Andreas, E. L., 2002: Parameterizing scalar transfer over snow and sea ice: A review. *J. Hydrometeorol*. **3**, 417–432.

Andreas, E. L, and B. B. Hicks, 2002: Comments on ‘‘Critical test of the validity of Monin–Obukhov similarity during convective conditions.’’ *J. Atmos. Sci*., **59**, 2605–2607, https://doi.org/10.1175/1520-0469(2002)059<2605:COCTOT>2.0.CO;2

Andreas, E. L, R. E. Jordan, and A. P. Makshtas, 2005: Parameterizing turbulent exchange over sea ice: The ice station Weddel results, *Bound.-Layer Meteor.*, **114**: 439–460.

Beljaars, A. C. M., 1995: The parametrization of surface fluxes in large-scale models under free convection. *Quart. J. Roy. Meteor. Soc*., **121**, 255–270.

Beljaars, A. C. M., A. R. Brown, and N. Wood, 2004: A new parametrization of turbulent orographic form drag. *Quart. J. Roy. Meteor. Soc.,* **130,** 1327-1347.

Benjamin, S. G., S. S. Weygandt, J. M. Brown, M. Hu, C. R. Alexander, T. G. Smirnova, J. B. Olson, E. P. James, D. C. Dowell, G. A. Grell, H. Lin, S. E. Peckham, T. L. Smith, W. R. Moninger, J. S. Kenyon, and G. S. Manikin, 2016: A North American hourly assimilation and model forecast cycle: the Rapid Refresh. *Mon. Wea. Rev.,* **144**, 1669–1694, doi:10.1175/MWR-D-15-0242.1.

Brutsaert, W., 1975: A theory for local evaporation (or heat transfer) from rough and smooth surfaces at ground level. *Water Resour. Res.,* **11**, 543-550.

Charnock, H., 1955: Wind stress on a water surface. *Quart. J. Roy. Meteor. Soc*., **81**, 639–640, doi:10.1002/qj.49708135027.

Chen F. and Y. Zhang, 2009: On the coupling strength between the land surface and the atmosphere: From viewpoint of surface exchange coefficients. *Geophys. Res. Lett*., **36**, L10404, doi:10.1029/ 2009GL037980.

Chen, Y., K. Yang, D. Zhou, J. Qin, and X. Guo, 2010: Improving the Noah land surface model in arid regions with an appropriate parameterization of the thermal roughness length. *J. Hydrometeor.*, **11**, 995–1006, https://doi.org/10.1175/2010JHM1185.1.

Cheng, Y., and W. Brutsaert, 2005: Flux-profile relationships for wind speed and temperature in the stable atmospheric boundary layer. *Bound.-Layer Meteor*., **114**, 519–538.

Davis, C., and Coauthors, 2008: Prediction of landfalling hurricanes with the advanced hurricane WRF model. *Mon. Wea. Rev.*, **136**, 1990–2005, https://doi.org/10.1175/2007MWR2085.1.

Deardorff, J. W., 1970: Convective velocity and temperature scales for the unstable planetary boundary layer and for Rayleigh convection. *J. Atmos. Sci.,* **27**, 1211–1213.

Deardorff, J. W., 1972: Parameterization of the planetary boundary layer for use in general circulation models. Mon. Wea. Rev., **100**, 93–106, https://doi.org/10.1175/1520-0493(1972)100%3C0093:POTPBL%3E2.3.CO;2

Donelan, M. A., B. K. Haus, N. Reul, W. J. Plant, M. Stiassnie, H. C. Graber, O. B. Brown, and E. S. Saltzman, 2004: On the limiting aerodynamic roughness of the ocean in very strong winds. *Geophys. Res. Lett.*, **31.** L18306, doi:10.1029/2004GL019460.

Dyer, A. J., and B. B. Hicks, 1970: Flux-gradient relationships in the constant flux layer. *Quart. J. Roy. Meteor. Soc.*, **96**, 715–721, https://doi.org/10.1002/qj.49709641012.

Edson, J. B. and Coauthors, 2013: On the exchange of momentum over the open ocean. *J. Phys. Oceanography.* **43**, 1589-1610.

Fairall, C. W., E. F. Bradley, J. E. Hare, A. A. Grachev, and J. B. Edson, 2003: Bulk parametrization of air–sea fluxes: Updates and verification for the COARE algorithm. *J. Climate*, **16**, 571–591.

Firl, G., L. Carson, L. Bernardet, D. Heinzeller, and M. Harrold, 2020. *Common Community Physics Package Single Column Model v4.1.0 User and Technical Guide*. 38pp. Available at https://dtcenter.org/GMTB/v4.1.0/scm-ccpp-guide-v4.1.0.pdf

Fitch, A. C., J. K. Lundquist, and J. B. Olson, 2013: Mesoscale influences of wind farms throughout a diurnal cycle. *Mon. Wea. Rev.*, **141**, 2173–2198, doi:10.1175/MWR-D-12-00185.1.

Foken, T., 2006: 50 years of the Monin–Obukhov similarity theory. *Bound.-Layer Meteor*., **119**, 431–447, https://doi.org/10.1007/s10546-006-9048-6.

Garratt, J. R., 1992: *The Atmospheric Boundary Layer*. Cambridge University Press, 316 pp.

Grachev, A. A., and C. W. Fairall, 1997: Dependence of the Monin–Obukhov stability parameter on the bulk Richardson number over the ocean. *J. Appl. Meteor*., **36**, 406–414, https://doi.org/ 10.1175/1520-0450(1997)036,0406:DOTMOS.2.0.CO;2.

Grachev, A. A., C. W. Fairall, and E. F. Bradley, 2000: Convective profile constants revisited. *Bound.-Layer Meteor.*, **94,** 495–515.

Green, B. W., and F. Zhang, 2013: Impacts of air–sea flux parameterizations on the intensity and structure of tropical cyclones. *Mon. Wea. Rev.*, **141**, 2308–2324, doi:10.1175/MWR-D-12-00274.1.

Harris, Lucas, L. Zhou, X. Chen, and J.-H. Chen, 2020: The GFDL Finite-Volume Cubed-Sphere Dynamical Core: Release 201912, GFDL Weather and Climate Dynamics Division Technical Memorandum. GFDL2020001. https://doi.org/10.25923/7h88-c534.

He, S., and Ohara, N., 2019: Modeling subgrid variability of snow depth using the Fokker-Planck equation approach. *Water Resources Research*, ***55***(4), 3137–3155. https://doi.org/10.1029/2017WR022017.

Jiménez, P. A., J. Dudhia, J. F. González-Rouco, J. Navarro, J. P. Montávez, and E. García-Bustamante, 2012: A revised scheme for the WRF surface layer formulation. *Mon. Wea. Rev*., **140**, 898–918, https://doi.org/10.1175/MWR-D-11-00056.1.

Kumar, P., and M. Sharan, 2012: An Analysis for the Applicability of Monin–Obukhov Similarity Theory in Stable Conditions. *J. Atmos. Sci.*, **69**, 1910–1915, https://doi.org/10.1175/JAS-D-11-0250.1.

Lee, E., E. Lee, and I. Choi, 2019: Impact of increased vertical resolution on medium-range forecasts in a global atmospheric model. *Mon. Wea. Rev.*, **147**, 4091–4106, https://doi.org/10.1175/MWR-D-18-0387.1.

Lee, T. R., and M. Buban, 2020: Evaluation of Monin-Obukhov and bulk Richardson parameterizations for surface-atmosphere exchange. *J. Appl. Meteor. Clim*., **59**, 1091-1107.

Li, Y., Z. Gao, D. H. Lenschow, and F. Chen, 2010: An improved approach for parameterizing turbulent transfer coefficients in numerical models. *Bound.-Layer Meteor*., **137**, 153–165.

Mahrt, L. T., and J. Sun, 1995: The subgrid velocity scale in the bulk aerodynamic relationship for spatially averaged scalar fluxes. *Mon. Wea. Rev.*, **123**, 3032–3041, https://doi.org/10.1175/1520-0493(1995)123<3032:TSVSIT>2.0.CO;2.

Mahrt, L. ,1998: Stratified atmospheric boundary layers and breakdown of models. *Theor. Comp. Fluid Dyn.*, **11**, 263–279, doi:10.1007/s001620050093.

Mahrt, L., 2007: Weak-wind mesoscale meandering in the nocturnal boundary layer. *Environ. Fluid Mech*., **7**, 331–347.

Mahrt, L., 2008: Bulk formulation of surface fluxes extended to weak-wind stable conditions. *Quart. J. Roy. Meteor. Soc*., **134**, 1–10.

Mahrt, L., 2010: Variability and maintenance of turbulence in the very stable boundary layer. *Bound.-Layer Meteor*., **135**, 1–18.

Monin, A. S., and A. M. Obukhov, 1954: Basic laws of turbulent mixing in the atmosphere near the ground. Tr. Geofiz. Inst., Akad. Nauk SSSR, **24**, 163–187.

Nakanishi, M. and H. Niino, 2009: Development of an improved turbulence closure model for the atmospheric boundary layer. *J. Meteor. Soc. Japan,* **87,** 895–912, doi:http://dx.doi.org/10.2151/jmsj.87.895.

Nieuwstadt, F. T. M., 1984: The turbulent structure of the stable, nocturnal boundary layer. *J. Atmos. Sci*., **41**, 2202–2216.

Niu, G.-Y., and Coauthors, 2011: The community Noah land surface model with multi-parameterization options (Noah-MP): 1. Model description and evaluation with local-scale measurements, *J. Geophys. Res.*, **116**, D12109, doi:10.1029/2010JD015139.

Olson, J. B., J. S. Kenyon, W. M. Angevine, J. M. Brown, M. Pagowski, and K. Sušelj, 2019: A description of the MYNN-EDMF scheme and coupling to other components in WRF-ARW. *NOAA Tech. Memo*. OAR GSD, **61**, 37 pp., https://doi.org/10.25923/n9wm-be49.

Paulson, C. A., 1970: The mathematical representation of wind speed and temperature profiles in the unstable atmospheric surface layer. *J. Appl. Meteor*., **9**, 857–861, https://doi.org/10.1175/1520-0450(1970)009,0857:TMROWS.2.0.CO;2.

Shin, H. H., S. Hong, and J. Dudhia, 2012: Impacts of the lowest model level height on the performance of planetary boundary layer parameterizations. *Mon. Wea. Rev.*, **140**, 664–682, https://doi.org/10.1175/MWR-D-11-00027.1.

Skamarock, W. C. and Coauthors, 2019: A description of the Advanced Research WRF version 4. NCAR Tech. Note NCAR/TN-556+STR, 162 pp. [Available online at http://www2.mmm.ucar.edu/wrf/users/docs/technote/v4_technote.pdf]

Smirnova, T. G., J. M. Brown, S. G. Benjamin, and J. S. Kenyon, 2016: Modifications to the Rapid Update Cycle Land Surface Model (RUC LSM) available in the Weather Research and Forecasting (WRF) model. *Mon. Wea. Rev.*, **144**, 1851–1865, https://doi.org/10.1175/MWR-D-15-0198.1.

Smith, S. D., 1988: Coefficients for sea surface wind stress, heat flux, and wind profiles as a function of wind speed and temperature. *J. Geophys. Res*., **93** (C12), 15 467–15 472.

Sorbjan, Z., 2006: Local structure of turbulence in stably stratified boundary layers. *J. Atmos. Sci*., **63**, 1526–1537.

Steeneveld, G. J., A. A. M. Holtslag, C. J. Nappo, B. J. H. van de Wiel, and L. Mahrt, 2008: Exploring the possible role of small-scale terrain drag on stable boundary layers over land. *J. Appl. Meteor.,* **47,** 2518-2530.

Steeneveld, G. J., Wokke, M. J. J., Groot Zwaaftink, C. D., Pijlman, S., Heusinkveld, B. G., Jacobs, A. F. G., and Holtslag, A. A. M., 2010: Observations of the radiation divergence in the surface layer and its implication for its parameterization in numerical weather prediction models, *J. Geophys. Res.*, **115**, D06107, doi:10.1029/2009JD013074.

Stensrud, D. J., 2007: *Parameterization schemes: Keys to understanding numerical weather prediction models*. Cambridge University Press, 450 pp.

Stull, R. B., 1988: *An Introduction to Boundary Layer Meteorology*. Kluwer Academic, 666 pp.

Sun, J., Takle, E. S., and Acevedo, O. C., 2020: Understanding physical processes represented by the Monin–Obukhov bulk formula for momentum transfer, *Bound.-Layer Meteor*., **177**, 69–95, https://doi.org/10.1007/s10546-020-00546-5.

Taylor, P. K., and M. J. Yelland, 2001: The dependence of sea surface roughness on the height and steepness of the waves. *J. Phys. Oceanogr.*, **31**, 572–590, https://doi.org/10.1175/1520-0485(2001)031<0572:TDOSSR>2.0.CO;2.

Tolman, H. L., 2008: User manual and system documentation of WAVEWATCH III version 3.14. NOAA/NWS/NCEP/MMAB Tech. Note 276, 220 pp. [Available online at http://polar.ncep.noaa.gov/mmab/papers/tn276/MMAB_276.pdf.]

Wei, H., M. Segal, W. J. Gutowski Jr., Z. Pan, R. W. Arritt, and W. A. Gallus Jr., 2001: Sensitivity of simulated regional surface thermal fluxes during warm advection snowmelt to selection of the lowest model layer height. *J. Hydrometeor*., **2**, 395–405.

Yang, K., T. Koike, H. Fujii, K. Tamagawa, and N. Hirose, 2002: Improvement of surface flux parameterizations with a turbulence-related length. *Quart. J. Roy. Meteor. Soc*., **128**, 2073– 2087.

Yang, K., and Coauthors, 2008: Turbulent flux transfer over bare-soil surfaces: Characteristics and parameterization. *J. Appl. Meteor. Climatol.*, **47**, 276–290, https://doi.org/10.1175/2007JAMC1547.1.

Yang, Z.-L., Niu, G.-Y., Mitchell, K. E., Chen, F., Ek, M. B., Barlage, M., Longuevergne, L., Manning, K., Niyogi, D., Tewari, M., and Xia, Y. (2011), The community Noah land surface model with multiparameterization options (Noah-MP): 2. Evaluation over global river basins, *J. Geophys. Res.*, **116**, D12110, doi:10.1029/2010JD015140.

Zängl, G., A. Gohm, and F. Obleitner, 2008: The impact of the PBL scheme and the vertical distribution of model layers on simulations of Alpine foehn. *Meteor. Atmos. Phys*., **99**, 105–128.

Zheng, W., H. Wei, Z. Wang, X. Zeng, J. Meng, M. Ek, K. Mitchell, and J. Derber, 2012: Improvement of daytime land surface skin temperature over arid regions in the NCEP GFS model and its impact on satellite data assimilation, *J. Geophys. Res*., **117**, 1-14, D06117, doi:10.1029/2011JD015901.

Zheng, W., M. Ek, K. Mitchell, H. Wei, and J. Meng, 2017: Improving the stable surface layer in the NCEP global forecast system. *Mon. Wea. Rev.*, **145**, 3969– 3987. https://doi.org/10.1175/mwr-d-16-0438.1

Zilitinkevich, S. S., 1995: Non-local turbulent transport: Pollution dispersion aspects of coherent structure of convective flows. Air Pollution Theory and Simulation, H. Power, N. Moussiopoulos, and C. A. Brebbia, Eds., Vol. I, *Air Pollution III, Computational Mechanics Publications*, 53–60.